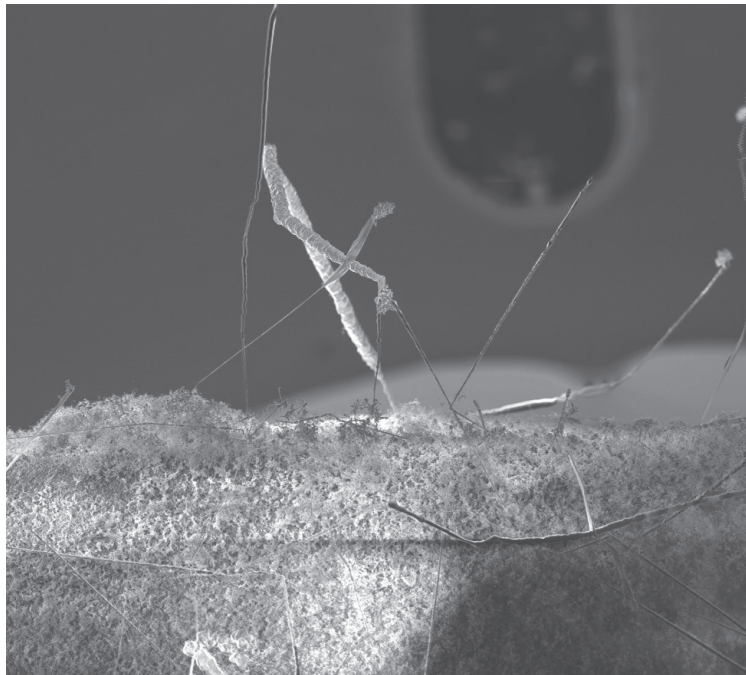




CHALMERS
UNIVERSITY OF TECHNOLOGY



High Temperature Oxidation of $\text{Mo}(\text{Si},\text{Al})_2$ composite in reducing atmosphere

Master's thesis in Master Programme Materials Chemistry and Nanotechnology

MARIA FORNMARK

MASTER'S THESIS 2015:NN

High Temperature Oxidation of $\text{Mo}(\text{Si},\text{Al})_2$ composite in reducing atmosphere

MARIA FORNMARK



Department of Chemistry and Chemical Engineering
Materials and Energy
Inorganic environmental chemistry
CHALMERS UNIVERSITY OF TECHNOLOGY
Gothenburg, Sweden 2015

High Temperature Oxidation of $\text{Mo}(\text{Si,Al})_2$ composite in reducing atmospheres
MARIA FORNMARK

© MARIA FORNMARK, 2015.

Supervisor: Kristina Hellström, Department of Chemistry and Chemical Engineering

Examiner: Professor Jan-Erik Svensson, Department of Chemistry and Chemical Engineering

Master's Thesis 2015:NN
Department of Chemistry and Chemical Engineering
Division of Energy and Materials
Inorganic Environmental Chemistry
Chalmers University of Technology
SE-412 96 Gothenburg
Telephone +46 31 772 1000

Cover: SEM image of the surface of an ER sample exposed for 24 hours in Argon, Nitrogen and Hydrogen.

Typeset in L^AT_EX
Printed by [Name of printing company]
Gothenburg, Sweden 2015

High Temperature Oxidation of Mo(Si,Al)₂ composite in reducing atmosphere
Maria Fornmark
Department of Chemistry and Chemical Engineering
Chalmers University of Technology

Abstract

MoSi₂ is a material commonly used as heating elements in high temperatures. In this project, exposures have been performed in 95% N₂ and 5% H₂ at 1600°C for 1, 24 and 168 hours. The material tested was a Mo(Si,Al)₂ composite, the commercial material also known as Kanthal Super ER. The aim of the project was to investigate the oxide formation and stability at low oxygen partial pressures as well as the impact of potential nitride formation on oxidation behaviour of Mo(Si,Al)₂-based materials. After exposure, the samples were investigated with XRD, SEM and EDX. It was found that AlN is formed during the initial oxidation stages, but after less than 24 hours this layer is overgrown with alumina and the nitride layer is found in the middle of the oxide layer. However, more statistics is needed to confirm these results. In addition, another exposure was performed, ER was exposed in 5% H₂, 47.5% N₂ and 47.5% Ar at 1600°C. This exposure showed similar results to the previous exposures, although it appeared more difficult for alumina to overgrow the nitride layer.

Keywords: MoSi₂, Mo(Si,Al)₂, Oxidation, Reducing atmosphere.

Acknowledgements

Thanks to Sandvik Heating Technology, who has supported this project. Also, thanks to Petter Lindblom and Erik Ström who took some of their precious time to show me around the site at Hallstahammar. I felt very welcome and learnt a lot. Thanks to Kristina Hellström for all the valuable help and for answering millions of stupid questions.

Thanks to all the people at Inorganic Environmental Chemistry for having me this semester and for all the fika. Especially thanks to the administrator Sandra Gustafsson for her friendly and helpful attitude.

Thanks to Professor Jan-Erik Svensson for good advice and for taking the time to read this report.

Thanks to all my lovely friends and family for your support when the light at the end of the tunnel felt far away. Every single lunch and fika took me one step closer to the finish line. Det var lätt!

Maria Fornmark, Gothenburg, December 2015

Contents

List of Figures	xi
List of Tables	xiii
1 Introduction	1
1.1 Background	1
1.2 MoSi ₂ : general properties and manufacturing	1
1.3 Low temperature oxidation	2
1.4 High temperature oxidation	3
1.5 Changing properties by alloying	3
1.6 Aim	5
2 Theory	7
2.1 Oxidation Reactions	7
2.2 Desired oxide properties	8
2.3 Stability of oxides	8
2.4 Oxidation Rate	10
2.5 Oxidation of Alloys	11
3 Methods	13
3.1 Sample preparation	13
3.2 Experimental Setup	14
3.3 Exposures	15
3.4 Characterisation methods	16
4 Results	17
4.1 Exposures at 1600°C in N ₂ /H ₂ atmosphere	17
4.1.1 Mass gain	18
4.1.2 XRD analysis	18
4.1.3 SEM cross section analysis	19
4.1.4 SEM surface analysis	21
4.1.5 EDX mapping	21
4.2 Exposure at 1600°C in N ₂ /H ₂ /Ar atmosphere	23
4.2.1 XRD analysis	24
4.2.2 SEM cross section analysis	24
4.2.3 SEM surface analysis	25
4.2.4 EDX mapping	26

5 Discussion	27
5.1 Conclusion	28
Bibliography	31
A Appendix I	I
A.1 Original XRD patterns	I

List of Figures

1.1	Phase diagram of Mo and Si[9].	2
1.2	Phase diagram of Mo, Si and Al at 1550°C[23].	4
1.3	Backscattered cross-section electron image of ER showing the different phases.	4
2.1	A schematic figure of the diffusion processes through the oxide scale.[25]	7
2.2	An example of an Ellingham diagram[27].	9
2.3	Weight gain versus time for commonly observed rate laws.[24]	10
2.4	Oxidation of alloys[27].	12
2.5	A backscattered SEM image of a cross section of pre-oxidised ER. . .	12
3.1	ER sample without alumina oxide layer.	13
3.2	Appearance of ER samples after preoxidising.	14
3.3	Backscattered electron image of ER sample after preoxidising. . . .	14
3.4	Schematic image of the experimental setup.	15
4.1	The images show the appearance of the ER samples before exposure (top left), after 1h (top right), 24 h (bottom left) and 168 h (bottom right) exposure respectively.	17
4.2	Mass gain per surface area (mg/cm^2) measured for ER samples. The circles represents the highest and lowest value measured.	18
4.3	XRD spectra of ER samples exposed 1h, 24h and 168h compared to preoxidised sample.	19
4.4	The left image shows a secondary electron image of an ER sample exposed for 1h. On the right is a backscattered electron image of the same sample.	19
4.5	The left image shows a secondary electron surface image of an ER sample exposed for 24h. On the right is a backscattered electron image of the same sample.	20
4.6	The left image shows a secondary electron surface image of an ER sample exposed for 168h. On the right is a backscattered electron image of the same sample.	20
4.7	The images show secondary electron surface images of ER samples exposed for 1, 24 and 168 hours respectively.	21
4.8	EDX mapping of a cross section from sample ER exposed for 1 hour.	22
4.9	EDX mapping of a cross section from sample ER exposed for 24 hours.	22
4.10	EDX mapping of a cross section from sample ER exposed for 168 hours.	23

4.11	ER before (left) and after (right) exposure for 24 h in argon, nitrogen and hydrogen	23
4.12	XRD analysis of ER exposed for 24 h in Argon, Nitrogen and Hydrogen, compared to preoxidised and not oxidised samples.	24
4.13	Cross section SEM images of ER after exposure for 24 h in argon, nitrogen and hydrogen. Left: Secondary electrons. Right: Backscattered electrons.	25
4.14	SEM surface images of ER after exposure for 24 h in argon, nitrogen and hydrogen. Left: Secondary electrons. Right: Backscattered electrons.	25
4.15	Secondary electron surface images of ER after exposure for 24 h in argon, nitrogen and hydrogen.	26
4.16	EDX mapping of a cross section from an ER sample exposed for 24 hours.	26
5.1	A scematic image of the oxide layers formed.	27
5.2	A stability diagram of AlN and Al ₂ O ₃ created in FactSage.	28
A.1	XRD pattern of ER exposed for 1 hour.	I
A.2	XRD pattern of ER exposed for 24 hours.	II
A.3	XRD pattern of ER exposed for 168 hours.	II

List of Tables

3.1	Table of the exposures performed.	15
4.1	Oxide thickness in μm measured from the SEM images above.	21

1

Introduction

1.1 Background

As technology advances there is a need for materials which can withstand even more challenging environments. For applications in the range of 800-1000°C, nickel based superalloys are suitable choices due to their excellent oxidation resistance and mechanical properties as well as their cost efficiency[1]. However, materials are also required which can operate at 1000-1600°C. In this temperature range, oxidation resistance becomes very important and possible materials are silicon-based ceramic materials, although these materials are brittle and are less cost efficient[1].

Disilicides are a group of materials having interesting properties of both metallic and ceramic materials. They are useful for technical applications in microelectronics, sensors and high temperature technology[2]. One example is MoSi₂, which has been used as a heating element material operating up to 1700°C. This is due to the high melting point and low density, and good thermal and electrical conductivity [3]. MoSi₂ based materials can be more reliable and less expensive than silicon-based ceramics. In addition, silicides are non-toxic and environmentally benign[1]. Attempts to develop this material has focused on high temperature strength and low temperature ductility[4], with the aim of improving the maximum operating temperature.

1.2 MoSi₂: general properties and manufacturing

MoSi₂ was discovered in 1907 and was initially used as a coating material, since the material was too brittle to be used as a structural material.[1]. The mechanical properties were investigated in 1950s and the pesting oxidation phenomenon was discovered, which is described further below. MoSi₂ has been used commercially for heating elements and the first patent was applied for in 1953 by Kanthal.

MoSi₂ has an excellent high temperature stability up to 1700°C due to the formation of a protective oxide scale of silica[2]. This layer acts as a barrier, protecting from further oxidation. This is why it is also investigated for structural applications. However, the oxidation behavior at lower temperatures is a challenge as well as the creep strength[1]. In addition, MoSi₂-based alloys have low fracture toughness and there is a problem of spallation of the oxide scale formed.

MoSi₂ is produced by stoichiometric mixing of Mo and Si, which is heated until Mo and Si reacts into MoSi₂[5]. The material is ground and mixed with a binder and

then extruded into rods. The rods are then sintered in high temperatures to increase density. As can be seen in the phase diagram in Figure 1.1, an excess of Si gives a pure Si phase, while an excess of Mo gives a Mo_5Si_3 phase[6]. This means that the the ratio of Mo and Si used affects material properties as an excess of Si lowers the melting point while an excess of Mo results in phase of Mo_5Si_3 in the material, promoting a faster oxidation[7, 8].

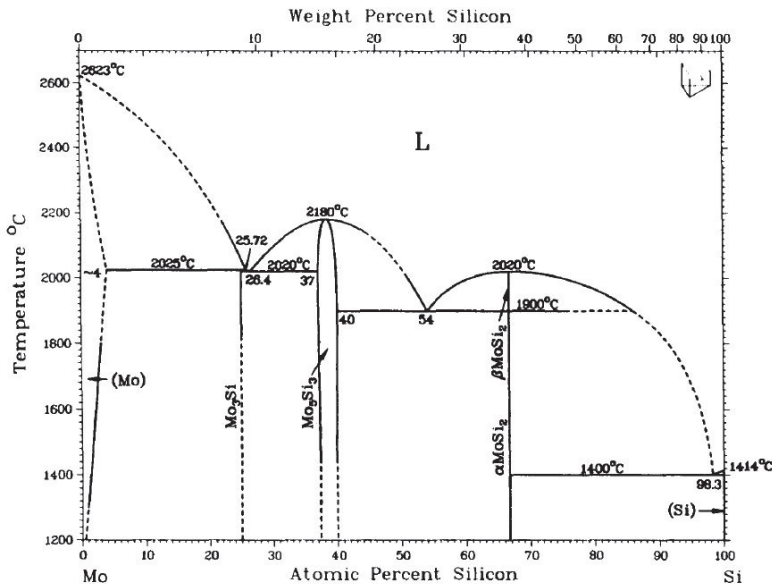


Figure 1.1: Phase diagram of Mo and Si[9].

1.3 Low temperature oxidation

At 400-700°C silicon and molybdenum are oxidized simultaneously, forming an oxide scale of MoO_3 and SiO_2 according to:



With sufficient vapour pressure MoO_3 evaporates, leaving a porous and non-protective oxide scale. This leads to an accelerated oxidation and the phenomenon called pesting. At higher temperatures a protective SiO_2 scale is formed which leads to a slower oxidation[3].

Previous research on the low temperature oxidation behavior of MoSi_2 have investigated the pesting mechanism in more detail and the influence of temperature, composition, porosity, partial pressure of oxygen and water vapour. Berkowitz-Mattuk[10], Meschter[7] and Chou[11] have performed studies revealing that the highest oxidation rate was found around 500°C.

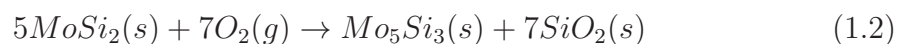
Another important aspect is the composition of the material. As mentioned earlier, MoSi_2 is not a homogeneous material as it also consists of Mo_5Si_3 phases or Si phases. These phases also affect the oxidation properties. Meschter[7] and Bertiss[8] found that the Mo_5Si_3 phase promotes faster oxidation. McKamey et. al[12] found that the material was provided protection from pesting with a slight excess of Si.

However, an excess of Si leads to a lower softening point of the material. In addition, Rubish[13] found that a more porous MoSi₂ material gave a more severe degradation and Berkowitz-Mattuk[10] found that the rate of disintegration was sensitive to the oxygen pressure while none was observed in the absence of O₂. Fitzer[14] investigated the influence of pO₂ and T and found that those parameters affected the oxidation behaviour significantly.

The oxidation behavior of MoSi₂ at lower temperatures has been investigated further by Hansson[15]. It was confirmed that MoSi₂ oxidises to MoO₃ and SiO₂. The oxidation is strongly influenced by the rate of Mo-removal from the oxide scale and the diffusion rate within SiO₂. The Mo removal is influenced by the exposure temperature and the water vapour concentration. Mo evaporation is slower in dryer atmospheres and lower temperatures. The diffusion rate within SiO₂ is dependent on the exposure temperature. At higher temperatures (550-700°C) the diffusion rate is fast enough to heal the pores left from Mo-evaporation and a pure SiO₂ scale can be formed, thus protecting the material underneath.

1.4 High temperature oxidation

Sharif[16] has investigated the high temperature oxidation behavior of MoSi₂ in the range of 1400°C to 1700°C. SiO₂ was formed and no spallation was observed. MoSi₂ has excellent oxidation properties up to 1700°C due to the formation of a protective SiO₂ layer. There are limited investigations at temperatures close to the melting temperature of the oxide. MoO₃ is initially lost from the oxide scale and this accelerates with increasing temperature. However, the increasing diffusivity of silicon within the oxide scale becomes high enough to heal the pores formed from volatilized MoO₃, creating a continuous Silica scale which is protective. This results in a lower oxidation rate[17]. The protective SiO₂ scale causes a decreased oxygen partial pressure at the scale/substrate interface, resulting in a selective oxidation of Si. This means that the substrate is depleted of Si and a Mo₅Si₃ phase is formed according to:



1.5 Changing properties by alloying

Heating elements often operate in a hostile environment due to the high temperatures and corrosive species present. In fact, the oxidation resistance is usually the limiting factor in high temperature applications and the most useful materials are those which form a protective oxide scale such as Al₂O₃, Cr₂O₃ and SiO₂[18]. There is a constant desire to improve materials to push the limits of how the materials can be used. The materials used are required to have mechanical properties as well as oxidation and corrosion resistance which are suitable for the environment they are going to operate in. The properties of MoSi₂ have been researched and changed by adding alloying elements such as Al and W[5]. By alloying, properties like fracture toughness and creep resistance have been significantly improved[19].

Aluminum can be added to the material, substituting silicon partly. These compounds form a stable alumina layer which do not suffer from volatilization and the high temperature strength is improved[20]. In addition, the thermal expansion coefficient of alumina and $\text{Mo}(\text{Si},\text{Al})_2$ is similar, which lowers the risk of spallation[21, 1]. Adding aluminum to MoSi_2 improves the oxidation behavior at low temperatures, but also the performance in low oxygen partial pressure when the temperature is high.

Figure 1.2 shows the phase diagram for Mo-Si-Al. It can be seen that the $\text{Mo}(\text{Si},\text{Al})_2$ phase has a narrow range. When manufactured, it is produced with an excess of Mo to avoid the liquid phase[22]. It can also be noted that relatively small amounts of aluminum promotes the hexagonal C40 structure.

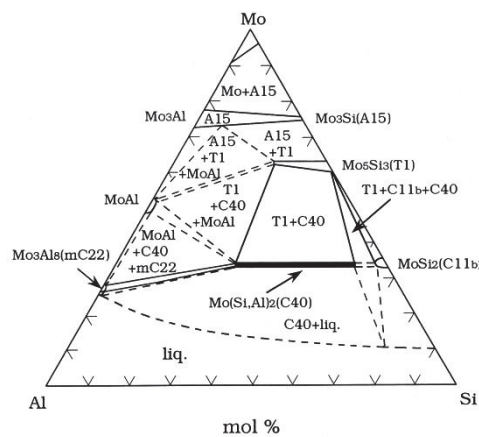


Figure 1.2: Phase diagram of Mo, Si and Al at 1550°C[23].

Figure 1.3 shows a cross section image of Kanthal Super ER, which is the commercial name for $\text{Mo}(\text{Si},\text{Al})_2$. The many differently colored areas shows that ER is a non-homogeneous material consisting of many phases. The dark parts are alumina, the grey areas are the bulk material $\text{Mo}(\text{Si},\text{Al})_2$ and the bright areas are Mo_5Si_3 .

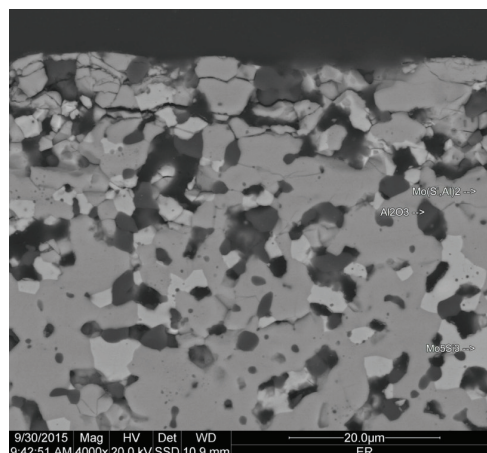


Figure 1.3: Backscattered cross-section electron image of ER showing the different phases.

1.6 Aim

This is a project initiated and supported by Sandvik Heating Technology. There is a demand from their customers for a material which is possible to use at reduced oxygen partial pressure and above 1600°C. Kanthal Super ER, which is a Mo(Si,Al)₂-based material, has been suggested since alumina is more stable than SiO₂.

The aim of the project was to investigate the oxide formation and stability at low oxygen partial pressures as well as the impact of potential nitride formation on Mo(Si,Al)₂-based materials. The material studied was the commercially available material Kanthal Super ER and the project involved performing exposures of the mentioned materials at Chalmers University of Technology, where the majority of the work was done, as well as a study visit during one week at Sandvik Heating Technology.

2

Theory

In the following sections, the basic theory behind the experiments conducted is presented. Firstly, the oxidation reactions are explained and important properties described. Then some aspects of thermodynamics and kinetics are described. The final section describes in short the complex mechanisms behind oxidation of alloys.

2.1 Oxidation Reactions

The general mechanisms of oxidation reactions are described by for example Jones[24]. When a metal surface is exposed to oxygen or another gas it reacts to form an oxide layer on the surface. Initially, the oxygen is adsorbed on the metal surface, and then the reaction takes place forming individual oxide nucleus. The oxide then grows to form a continuous film and finally the oxide thickens.

Depending on the properties of the oxide formed, it can protect the metal surface from further oxidation, by acting as a barrier between the metal surface and the surroundings thus slowing down the oxidation. This is important for high temperature applications as it affects the lifetime of components.

When the whole surface is covered with an oxide scale and the surface is separated from the gas, the oxidation reaction is dependent on diffusion of the reactants through the oxide scale. The oxide can grow either inwards or outwards depending on the diffusion. For oxide to grow outwards, metal cations must diffuse through the oxide. The opposite happens for an inward growing oxide, oxygen anions diffuse through the oxide to the oxide/metal interface. This is illustrated in Figure 2.1

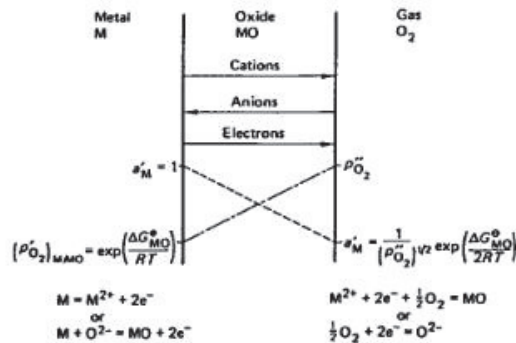


Figure 2.1: A schematic figure of the diffusion processes through the oxide scale. [25]

Diffusion rate is mainly determined by imperfections in the material, but also by the presence of pores and micro-channels. However, a porous oxide is not a good protection for the material beneath.

2.2 Desired oxide properties

For an oxide to be useful as protection against further oxidation, the following properties are desirable[24]:

- Good adherence to prevent flaking and spallation.
- High melting point.
- Low vapour pressure to avoid evaporation.
- Oxide film and metal should have similar thermal expansion coefficient.
- Low electrical conductivity and low diffusion coefficients for metal ions and oxygen.

2.3 Stability of oxides

The thermodynamics of oxides has been explained by many, for example Jones[24] and Birks[27]. In thermodynamics, the possibility of a reaction to happen is determined by the second law of thermodynamics which is described by the equation:

$$\Delta G^0 = \Delta H^0 - T\Delta S^0 \quad (2.1)$$

If ΔG^0 is negative it is possible for the reaction to happen spontaneously for the reactants at standard state. ΔH^0 is the standard enthalpy of formation (kJ/mol), ΔS^0 (J/mol*K) is the standard entropy of formation and T is the temperature in K. The values of these are specific for each reaction and fairly constant at changing temperatures. This means that ΔG^0 plotted as a function of T is approximately a straight line.

An Ellingham diagram, where ΔG^0 for many reactions is plotted as a function of T, is shown in figure 2.2. This diagram can be used to compare the stability of oxides at different temperatures at standard state ($p_{O_2}=1$ atm). A lower position on the diagram means a lower free energy of formation, and a more stable oxide.

However, when the reactions occur at non-standard state the case is different. For the general reaction



the free energy ΔG changes according to:

$$\Delta G = \Delta G^0 + RT \ln \frac{a_C^c a_D^d}{a_A^a a_B^b} \quad (2.3)$$

At equilibrium $\Delta G = 0$ and the equation becomes

$$\Delta G^0 = -RT \ln \frac{a_C^c a_D^d}{a_A^a a_B^b} \quad (2.4)$$

For the simple oxidation reaction



where M is a metal, equation 2.4 becomes

$$\Delta G^0 = RT \ln p_{O_2} \quad (2.6)$$

Here, the activity for oxygen is assumed to be equal to the partial pressure, and the activity for solid reactants is defined as unity.

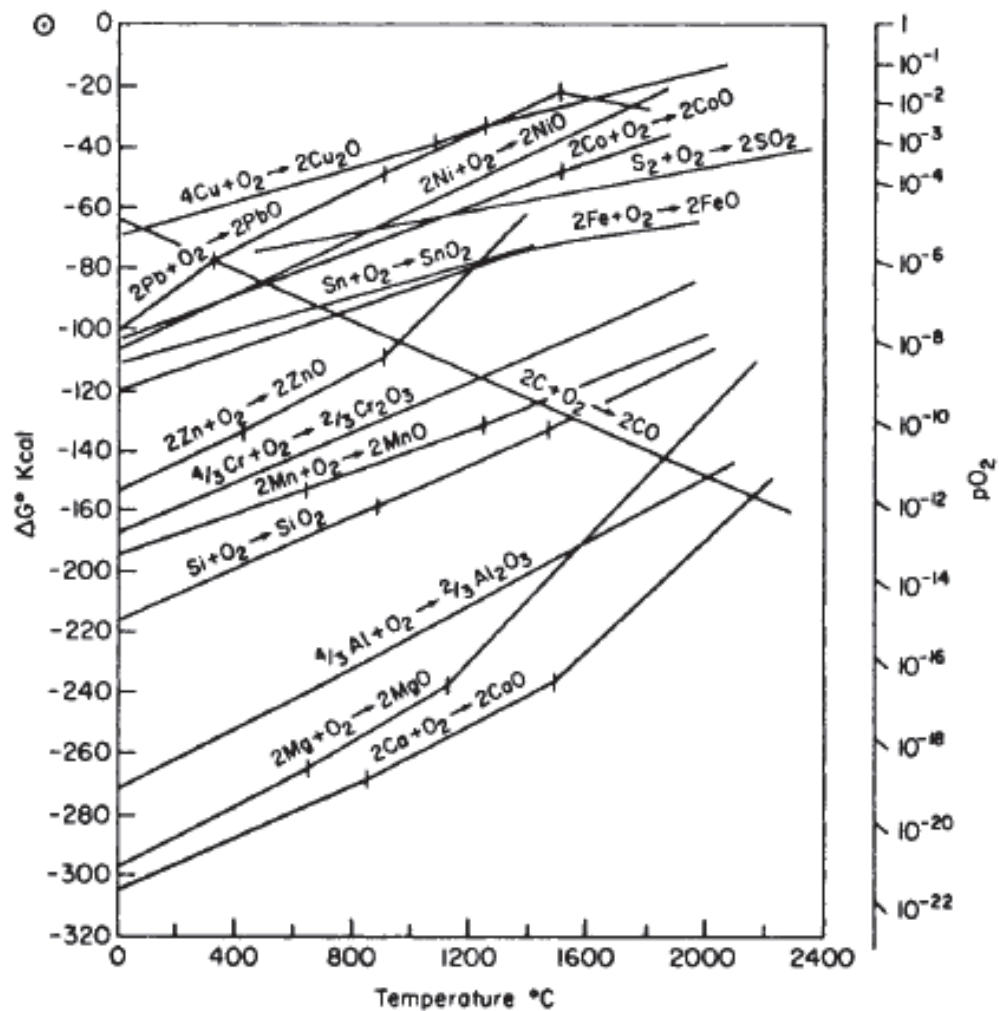


Figure 2.2: An example of an Ellingham diagram[27].

This means that there is a characteristic equilibrium oxygen partial pressure for the dissociation of any oxide. A p_{O_2} below this critical value will reduce the oxide to

pure metal. This value can also be determined from the Ellingham diagram by using the axis on the right side, and extending a straight line from the point marked O. However, thermodynamics has its limits as it can only predict if a reaction is possible or not. The Ellingham diagram cannot be used to determine the rate of reactions. That is why kinetics must also be studied.

2.4 Oxidation Rate

The rate of oxidation growth is studied by collecting data of weight gain at different times of exposure[26]. The surface reaction with oxygen causes the sample to gain weight which corresponds to a thicker oxide layer. There are three normal models describing oxidation growth, the parabolic rate law, the linear rate law and the logarithmic rate law. Figure 2.3 shows weight gain as a function of time for the different rate laws.

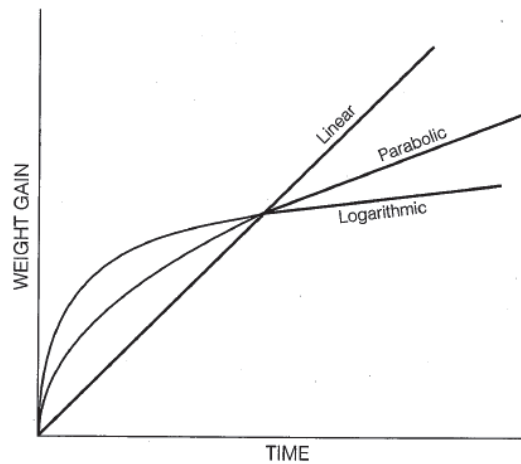


Figure 2.3: Weight gain versus time for commonly observed rate laws.[24]

The parabolic rate law is applicable when diffusion is the rate controlling mechanism. According to Birks[27], a number of assumption has to be valid in order for the parabolic rate law to be accurate:

- Product layer is compact and perfectly adherent.
- Migration of ions or electrons across the scale is the rate controlling process.
- Thermodynamic equilibrium is established at both metal scale and scale-gas interface.
- The scale shows only small deviations from stoichiometry.
- Thermodynamic equilibrium is established locally throughout the scale.
- The scale is thick compared to distances over which space charge effects occur.
- Neglecting non-metal solubility in the metal.

With these assumptions the parabolic rate law is derived from Fick's law, assuming steady-state and constant diffusivity D .

$$\frac{dx}{dt} = CD \frac{\delta c}{x} \quad (2.7)$$

where dx/dt is the rate of scale thickening, C is a proportionality constant, D is the diffusivity and δc is the concentration gradient. Integrating this equation and putting $k_p = CD\delta c$ gives the parabolic relationship

$$x^2 = k_p t \quad (2.8)$$

Since weight gain is proportional to oxide thickness, x can be substituted for mass gain, Δm . For convenience, Δm^2 is usually plotted as a function to t , to give a straight line if the parabolic rate law is obeyed. The parabolic rate law is the most common model used for high temperature oxidation.

A linear rate law applies when a reaction is rate controlling, meaning that the transport through the oxide is fast. Usually this is due to a non-protective oxide, but it could also appear at low partial pressure of O_2 . A logarithmic rate law is most common for low temperatures and thin films.

Often, the reality is more complicated than these rate laws. The parabolic rate law may not apply in early stages, before the oxide is thick enough and covers the whole surface. Multiple oxide phases may also change the behaviour of oxide growth.

2.5 Oxidation of Alloys

When a multicomponent alloy is exposed to many reactive gas components, it is a complex task to determine what will happen. Oxidation of alloys is more complex than oxidation of pure metals for many different reasons[27]:

- The different metals will have different affinities for oxygen reflected by the difference in free energy of formation of the oxides.
- Ternary and higher oxides may be formed.
- A degree of solid solubility between the oxides may exist.
- The various metal ions will have different mobilities in the oxide phases.
- The various metals will have different diffusivities in the alloy.
- Dissolution of oxygen into the alloy may result in sub-surface precipitation of oxides of one or more alloying elements (internal oxidation)

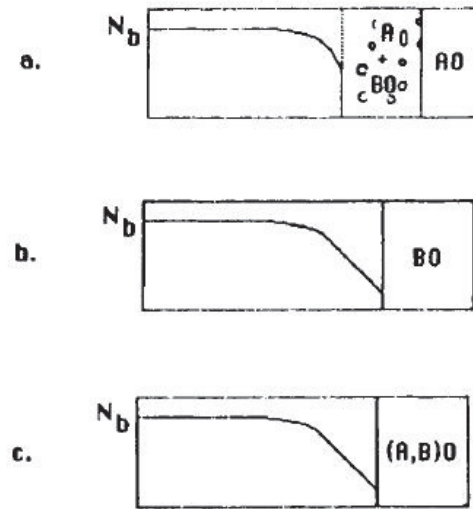


Figure 2.4: Oxidation of alloys[27].

The oxide scale formed on an alloy depends on the solubility and the concentration of the components. Figure 2.4 shows three different cases for an alloy consisting of components a and B, where the oxide of B is more stable. In the case showed in (a), the concentration of B is low and an oxide layer AO is formed together with internal oxidation of B. In the (b) case the concentration of B is high enough to form an oxide layer of BO instead. This is the desired case for corrosion resistance. The (c) image shows what can happen when the solubility of the components are simliar. However, as BO is formed the material beneath is depleted of B leading to en enriched phase of A. This effect can be seen in figure 3.3, which shows ER untreated and preoxidised for 5 minutes. The dark layer on top is Al₂O₃ and the white layer below is Mo₅Si₃ which is formed when Mo(Si,Al)₂ is depleted of Al. As can be seen in Figure 1.3, none of these layer are present in the non-treated ER.

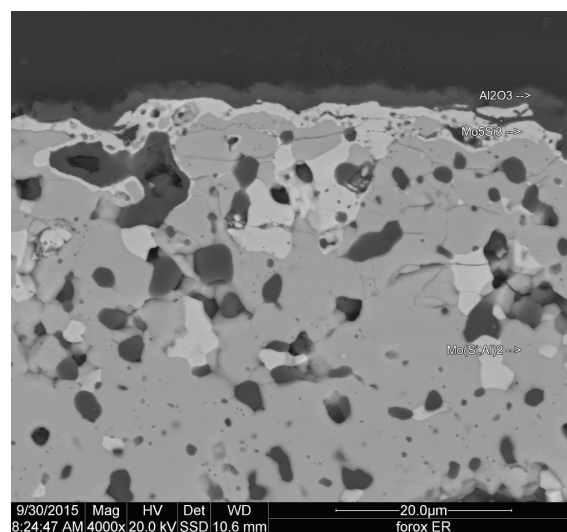


Figure 2.5: A backscattered SEM image of a cross section of pre-oxidised ER.

3

Methods

This section describes the materials and experimental methods used during this project. Firstly, a description of the samples used and the preparation methods is presented. Secondly, a description of the experimental setup is provided with an overview of the exposures performed. Finally, the characterisation methods used are described and presented.

3.1 Sample preparation

Kanthal Super ER is a commercially available material that is based on $\text{Mo}(\text{Si},\text{Al})_2$. Samples were received as rods with 6 mm diameter from Sandvik Heating Technology, with the density 5.40 g/cm^3 . The rods were ground to remove the outer oxide layer remaining from the sintering process and then cut in to pieces of roughly 25 mm. The end parts of the samples were ground with 180 GRIT SiC papers and then the samples were washed ultrasonically with distilled water, acetone and ethanol for 10 minutes respectively. Afterwards, the samples were dried in air. Finally the samples were weighed using a microbalance with a precision of $1 \mu\text{g}$. The appearance of the samples after washing is showed in Figure 3.1. The samples were pre-oxidised during 5 minutes in air at 1450°C , ramping up for 28 minutes, the result is shown in Figure 3.2. After pre-oxidation, the samples were weighed again. Figure 3.3 shows ER in SEM after preoxidation, and an oxide layer of about $2.3 \mu\text{m}$ can be observed.



Figure 3.1: ER sample without alumina oxide layer.



Figure 3.2: Appearance of ER samples after preoxidising.

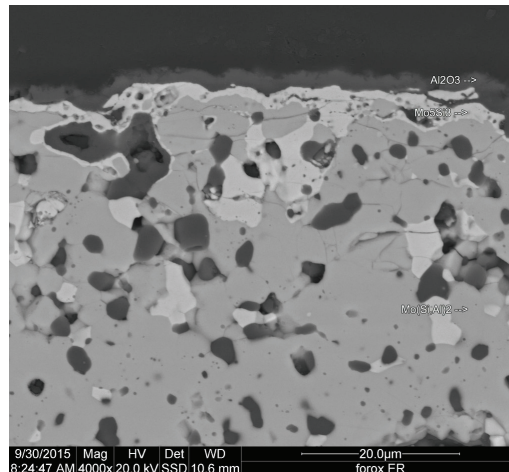


Figure 3.3: Backscattered electron image of ER sample after preoxidising.

3.2 Experimental Setup

The experimental setup was built according to the schematic picture in Figure 3.4. The furnace used was a horizontal tube furnace fitted with an alumina tube. The samples were placed inside the tube which was then sealed with glass pieces. The temperature of the furnaces were checked in advance with an external thermo couple to determine the location of the hottest zone of the tube and also to calibrate the temperature regulator of the furnace. The partial pressure of oxygen prior to adding hydrogen gas was measured to be approximately 9 ppm using a lambda sensor, Rapidox 2100ZF Oxygen Analyser. The theoretical equilibrium partial pressure of H_2O and O_2 after adding H_2 was calculated by using the software FactSage and was determined to be $1.7994 \cdot 10^{-5}$ atm and $1.3783 \cdot 10^{-15}$ atm respectively. This corresponds to a dew point of $-56^\circ C$ and $1.37 \cdot 10^{-9}$ ppm O_2 .

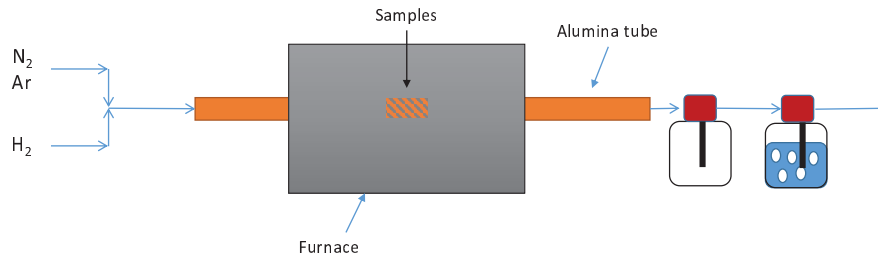


Figure 3.4: Schematic image of the experimental setup.

The experimental setup was built to be able to provide a gas mixture with a dew point of 0 or -56°C . Dew point -56°C was received by running the gas dry and 0°C was received by running the gas through a membrane which provided moisture to the gas flow. However, due to limit of time, only exposures in dew point -56°C were conducted.

3.3 Exposures

The furnace was flushed with N_2 at least 7 hours, usually overnight, before starting an exposure in order to get rid of as much oxygen as possible. The furnace was programmed to ramp up the temperature at an indicated range and then hold the target temperature for an indicated time. Afterwards, the temperature ramps down and then the furnace shuts off. Two samples were run in each exposure, and all exposures were repeated except for the exposure for 168 hours due to limited time frame. The Table 3.1 shows the exposures performed. As the gas mixture of 95% N_2 and 5% H_2 is commonly used in the industry it was chosen for most of the exposures. The exposure with argon was conducted out of curiosity what would happen at an even lower dew point, and the dew point was calculated to -65°C .

Table 3.1: Table of the exposures performed.

Exposure	Sample	Atmosphere	Dp ($^{\circ}\text{C}$)	Gas flow (ml/min)	Temperature ($^{\circ}\text{C}$)	Ramp ($^{\circ}\text{C}/\text{min}$)	Duration (h)
1	ER	5% H_2 47.5% N_2 47.5% Ar	-65	200	1600	10	24
2	ER	5% H_2 95% N_2	-56	200	1600	10	1
3	ER	5% H_2 95% N_2	-56	200	1600	10	24
4	ER	5% H_2 95% N_2	-56	200	1600	10	168

3.4 Characterisation methods

XRD analysis was used to examine the phases of the surface of the samples. A Siemens D5000 X-ray diffractometer was used, with a Cu-K α source with a wavelength of 1.5418 Å. An incident angle of 1° was used in order to avoid too dominant peaks from the base material. After studying the work of Linda Ingemarsson[5], the scan was made over the 2 θ range 10-70°.

In order to examine the microstructure and quantitatively identify elements present in the samples, scanning electron microscope (SEM) was used. The equipment was a FEI Quanta 200 environmental scanning electron microscope (ESEM). For EDX (Energy Dispersive X-ray spectrometry) an Oxford Inca EDX was used, which was installed on the ESEM and the accelerating voltage was 20 kV.

The basic principle behind SEM is that electrons are accelerated towards the sample, and the reflected electrons are detected to create an image. Two types of detectors were used in this case. The ETD detector detected secondary electrons, which are electrons that have been knocked out from the sample by the incident beam. These electrons have low energy, and only the ones coming from the surface will reach the detector. That is why an image generated by secondary electrons shows the surface topography. The second detector used was the SSD detector, which detects backscattered electrons. These electrons are scattered electrons from the incident beam. Areas with high average atomic number produce more backscattered electrons and appear brighter in the image.

An EDX detector detects X-rays generated when the electron beam hits the sample. As each element generates a specific characteristic wavelength, EDX can be used to identify the phases present in a sample. Therefore this was a useful method when analysing the Mo(Si,Al)₂ as those samples consist of many phases.

In the ESEM, both the surface and the cross section of the samples were analyzed. Cross section samples were prepared by embedding them in epoxy and then polished down to 1 μ m diamond suspension. Afterwards they were painted with silver color in order to avoid charging effects from non-conducting phases i. e. oxides. Finally, the samples were sputtered with gold for 30 seconds.

4

Results

In this section, results from the exposures performed are presented. The main results are presented in section 4.1, where exposures have been performed in 1600°C and N₂/H₂ atmosphere. In addition, a additional exposure in Ar/N₂/H₂ was performed and these results are presented below in a separate section.

4.1 Exposures at 1600°C in N₂/H₂ atmosphere

Figure 4.1 shows the appearance of the unexposed ER samples as well as after 1, 24 and 168 hours of exposure. The preoxidised sample has a grey colour which is expected as a layer of alumina should form. However, the samples exposed for 1 and 24 hours have a white color, while the 168 hour sample is gray like the preoxidised sample, but covered in a thin layer of white dust. The white powder appears to be falling off, which can be observed as there are white stains on the plate where the samples had been resting inside the furnace. Another interesting feature of all the exposed samples is the white needles growing out from the surface, which are larger after a longer time of exposure.

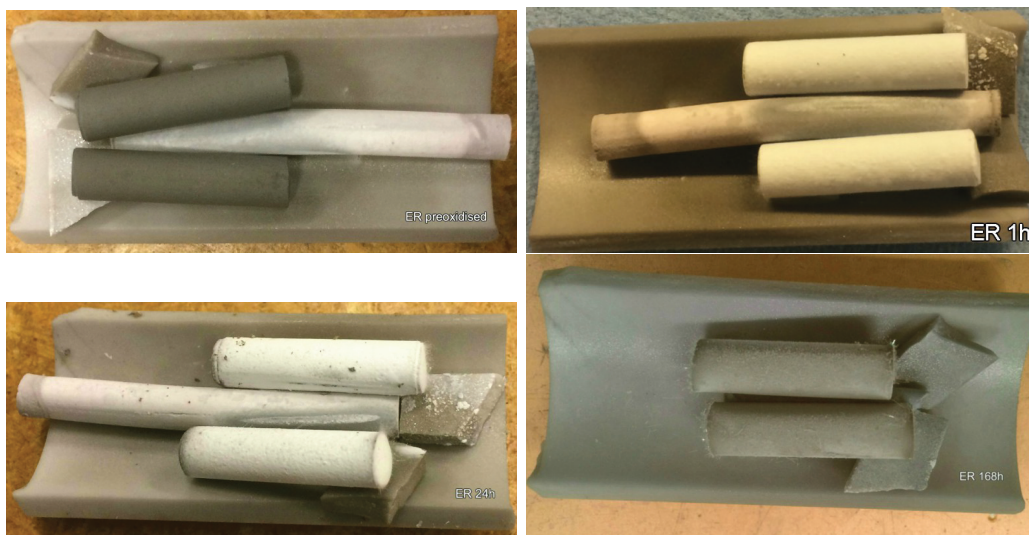


Figure 4.1: The images show the appearance of the ER samples before exposure (top left), after 1h (top right), 24 h (bottom left) and 168 h (bottom right) exposure respectively.

After the exposures, a grey deposit was found on the outlet side of the alumina

tube. This deposit was analysed in both XRD and SEM and appears to consist of amorphous SiO_2 . Apparently, a volatile specie is formed in the tube and deposited on the inside when it reaches cooler parts of the tube. There were no signs which could help indicate if the deposit comes from the samples or the tube itself.

4.1.1 Mass gain

Figure 4.2 shows mass gain per surface area as a function of time for ER samples. The surface area was calculated from knowing the density and the sample diameter together with the mass of the unexposed samples, which was noted before any exposure for all samples. The mass gain curve is sub-parabolic, indicating a protective oxide scale. However, it should be noted that three data points are not enough to draw any conclusions.

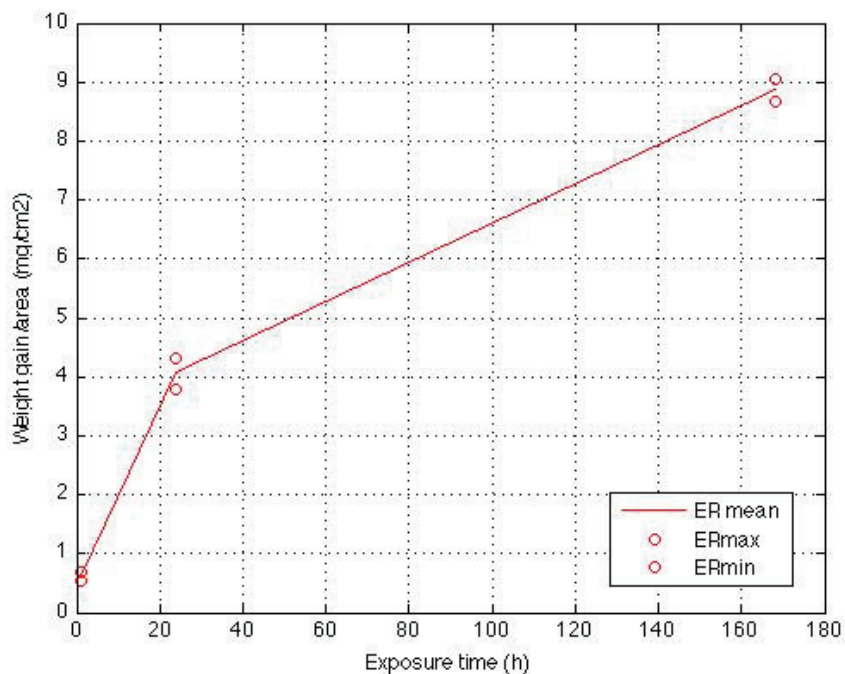


Figure 4.2: Mass gain per surface area (mg/cm^2) measured for ER samples. The circles represents the highest and lowest value measured.

4.1.2 XRD analysis

Figure 4.3 shows the XRD spectra for the ER samples exposed for 1, 24 and 168 hours compared to the preoxidised samples. The peaks for the bulk material and Mo_5Si_3 phase disappear as the oxide layer thickens and the alumina peaks grow larger. Peaks for AlN show up already after 1 hour of exposure and grow larger after 24 hours. However, after 168 hours the alumina peaks are clearly dominant, although small peaks for AlN can be found by looking closely. These results indicate that AlN initially forms on the surface, but stops forming after a certain time of exposure.

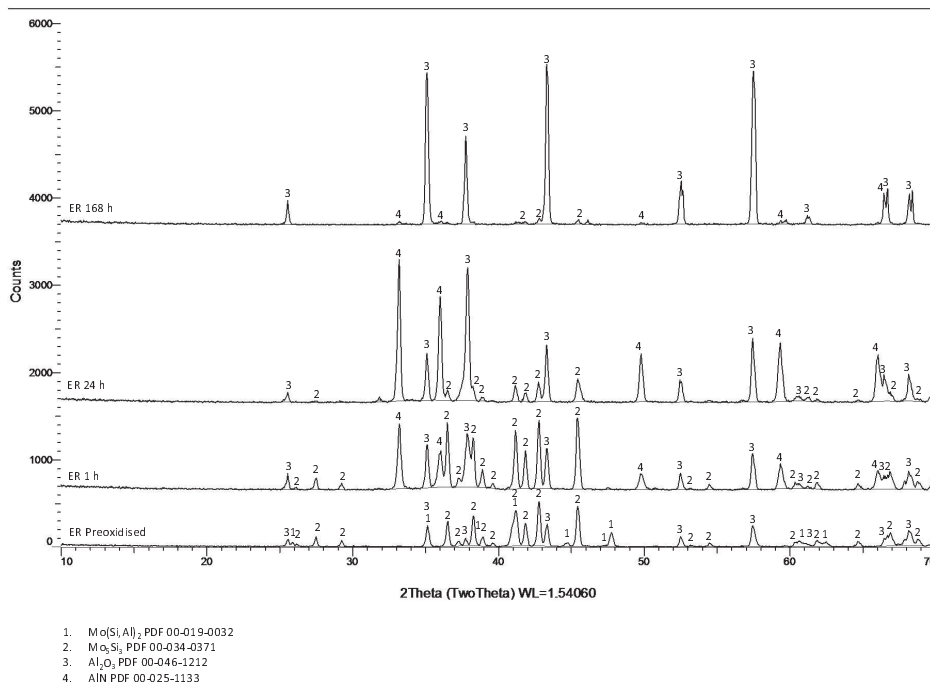


Figure 4.3: XRD spectra of ER samples exposed 1h, 24h and 168h compared to preoxidised sample.

4.1.3 SEM cross section analysis

Figure 4.4, 4.5 and 4.6 shows SEM images of ER samples in cross section. A dark oxide layer can be observed on top, which consists of Al₂O₃. Beneath is a brighter layer which is Mo₅Si₃, resulting from depletion of aluminum as the oxide layer forms and the Mo₅Si₃/Al₂O₃ thickness ratio is constant and independent of exposure time. It can also be observed that the Mo₅Si₃ phase becomes more and more porous with longer exposure time. This is due to the aluminium depletion of the material and that Mo₅Si₃ has higher density and lower volume than MoSi₂.

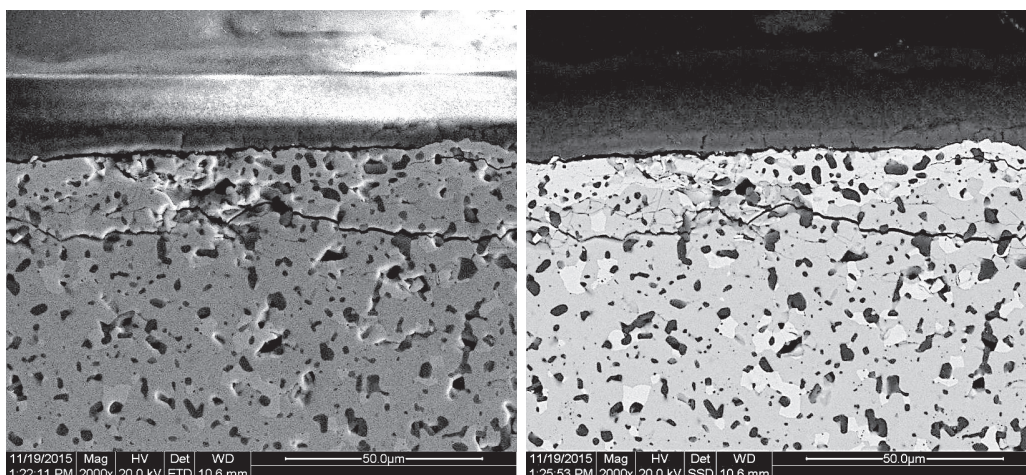


Figure 4.4: The left image shows a secondary electron image of an ER sample exposed for 1h. On the right is a backscattered electron image of the same sample.

4. Results

After 1 h a tiny oxide layer, about $4\mu\text{m}$ thick, can be seen and on top is a more porous layer, which is difficult to distinguish from the background. Moreover, after 24 h the porous oxide layer appears to be gone and the more dense oxide layer is thicker, now about $29\mu\text{m}$. However, the top part of the oxide layer looks more porous and rough. The bright Mo_5Si_3 layer has grown significantly thicker.

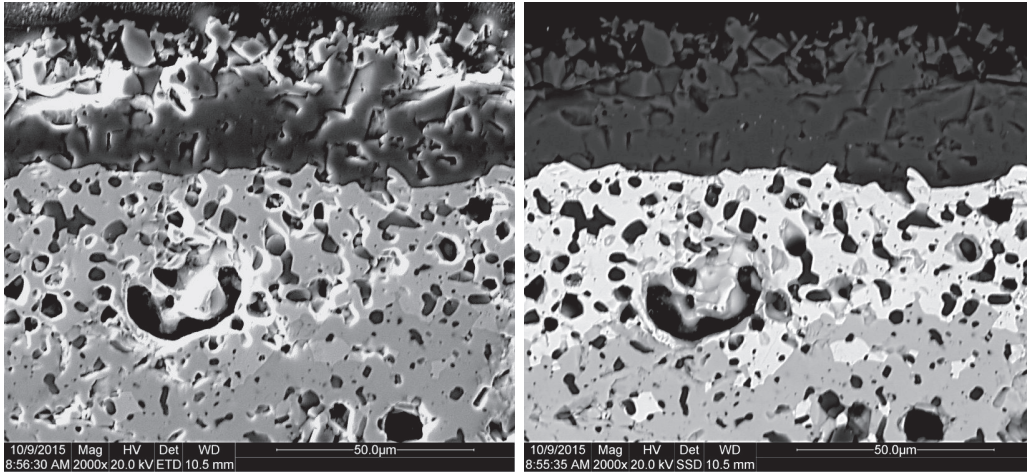


Figure 4.5: The left image shows a secondary electron surface image of an ER sample exposed for 24h. On the right is a backscattered electron image of the same sample.

In Figure 4.6, it can be seen that the oxide layer and the Mo_5Si_3 phase have grown much thicker after 168 hours as the oxide layer is now about $52\mu\text{m}$. This is primarily seen by noting the magnification of the images, which is much lower. The oxide layer is dense and smoother than before, except for the middle part, which is more porous. The Mo_5Si_3 is also clearly more porous than before, and much more porous than the bulk material, as expected.

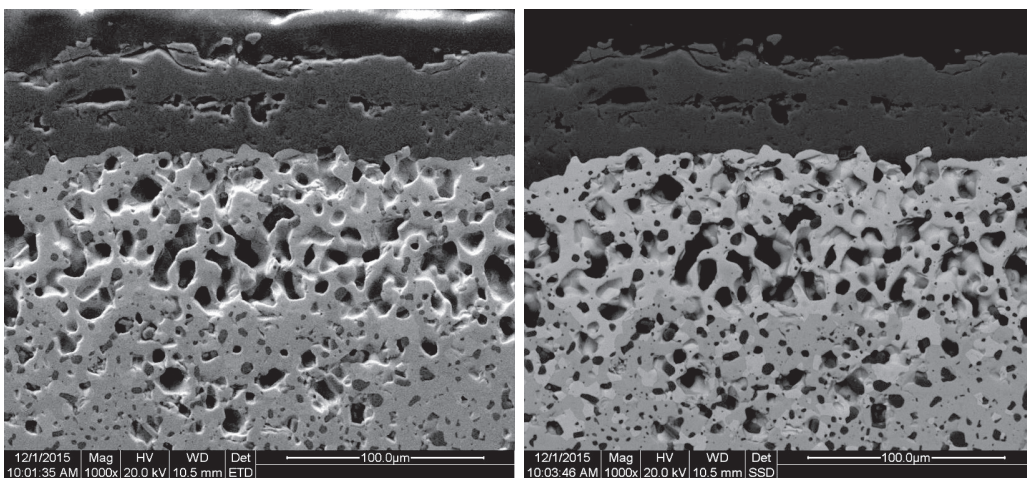


Figure 4.6: The left image shows a secondary electron surface image of an ER sample exposed for 168h. On the right is a backscattered electron image of the same sample.

Table 4.1 shows the oxide thickness measured from the images above. It gives a rough idea of how fast the layer is growing. These numbers can be compared to the work of Ingemarsson[20], where 50 μm of oxide was observed after exposure in 1600°C for 72 hours in dry air. In Table 4.1 it can be seen that 50 μm oxide is formed after 168 hours, which indicates that the oxide formation is much slower in this case.

Table 4.1: Oxide thickness in μm measured from the SEM images above.

Sample	Preox	1 h	24 h	168 h
ER	2.3	4.3	29	52

It was also discovered that on top of the alumina layer was a layer of AlN, which is the white powder covering some samples. This layer not visible in the SEM images as it was discovered that it was dissolved during the sample preparation process. To check that the top layer was indeed AlN, it was scraped off one of the samples and analysed in XRD. Due to this mistake, there are no indications on how much of the nitride is formed, which is unfortunate.

4.1.4 SEM surface analysis

Figure 4.7 shows SEM surface images of ER samples. After 1 h, the porous surface seen in Figure 4.4 can be observed as a network of tiny rods and it was hard to focus in the microscope as there were many layers. After 24 h the surface looks different. Although the surface is still porous, it is more flat and new structures have appeared. Similar structures are covering the whole surface after 168 hours and a more flat surface can be seen beneath. EDX analysis gave no clear answers. For the 1 and 24 hours sample, the whole surface appeared to consist of Al, N and O in similar proportions no matter where the point was taken and the 168 hours sample indicated only Al and O.

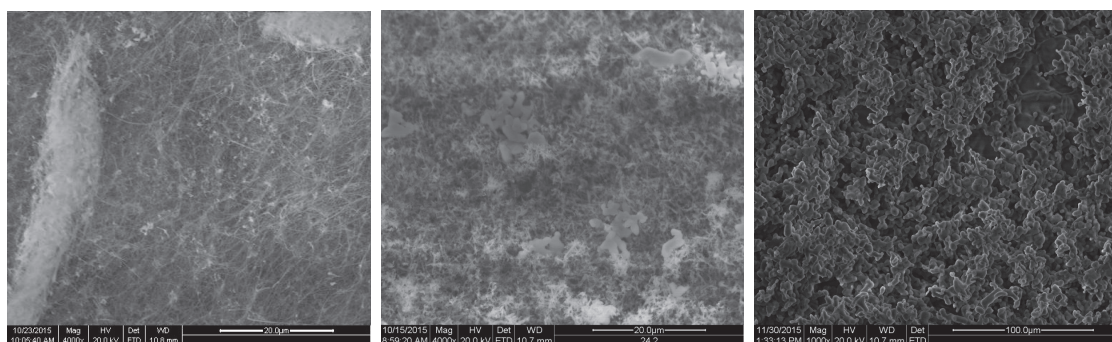


Figure 4.7: The images show secondary electron surface images of ER samples exposed for 1, 24 and 168 hours respectively.

4.1.5 EDX mapping

Figure 4.8 shows EDX mapping of ER exposed for 1 hour. The porous layer on top appears to consist of mainly Al_2O_3 and the nitride AlN is mainly located on top of

4. Results

the more dense oxide layer. In addition, the Mo_5Si_3 phase beneath the oxide layer and the bulk material can be clearly distinguished.

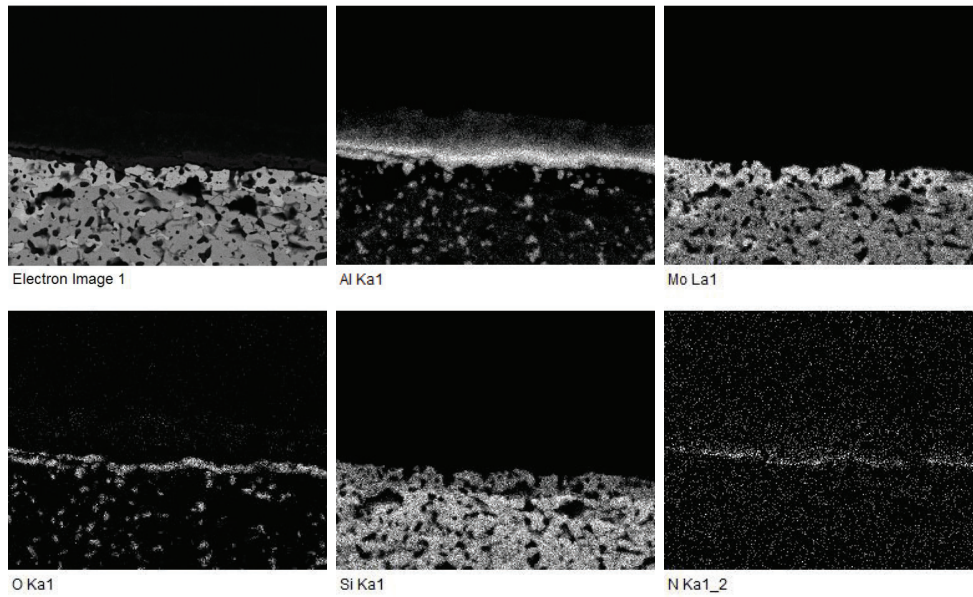


Figure 4.8: EDX mapping of a cross section from sample ER exposed for 1 hour.

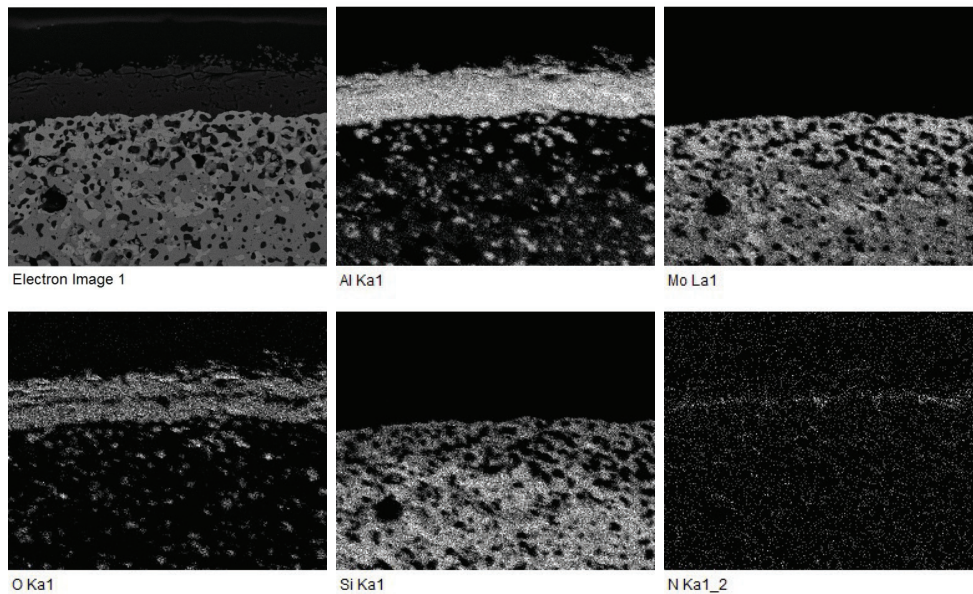


Figure 4.9: EDX mapping of a cross section from sample ER exposed for 24 hours.

Figure 4.9 show that there is now a thicker oxide scale of Al_2O_3 . The nitrogen layer is now located in the middle of the oxide layer, and there is also less oxygen in the same region. Figure 4.10 shows that the situation is similar after 168 hours, again the nitrogen layer is located in the middle of the oxide.

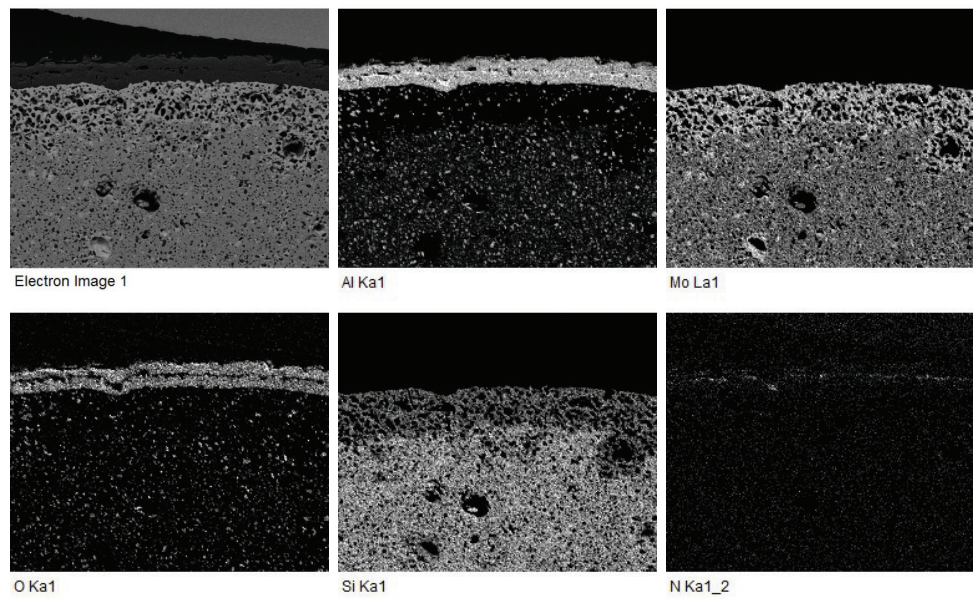


Figure 4.10: EDX mapping of a cross section from sample ER exposed for 168 hours.

4.2 Exposure at 1600°C in N₂/H₂/Ar atmosphere

Figure 4.11 shows the result from the exposure of ER in argon, nitrogen and hydrogen. To the left is the unexposed preoxidised sample, and to the right is the sample after 24 hours of exposure. It can be seen that after 24 hours of exposure, the samples are covered with a white powder and white needles have grown out from the sample. In addition, the samples had grown together and were impossible to separate.



Figure 4.11: ER before (left) and after (right) exposure for 24 h in argon, nitrogen and hydrogen

4.2.1 XRD analysis

Figure 4.12 shows the XRD analysis of the samples. As can be seen, Mo_5Si_3 and $\text{Mo}(\text{Si},\text{Al})_2$ peaks disappear or are much less visible after exposure. The Al_2O_3 peaks grow as the sample is exposed for a longer time, and after the exposure for 24 hours dominant peaks of AlN have shown up.

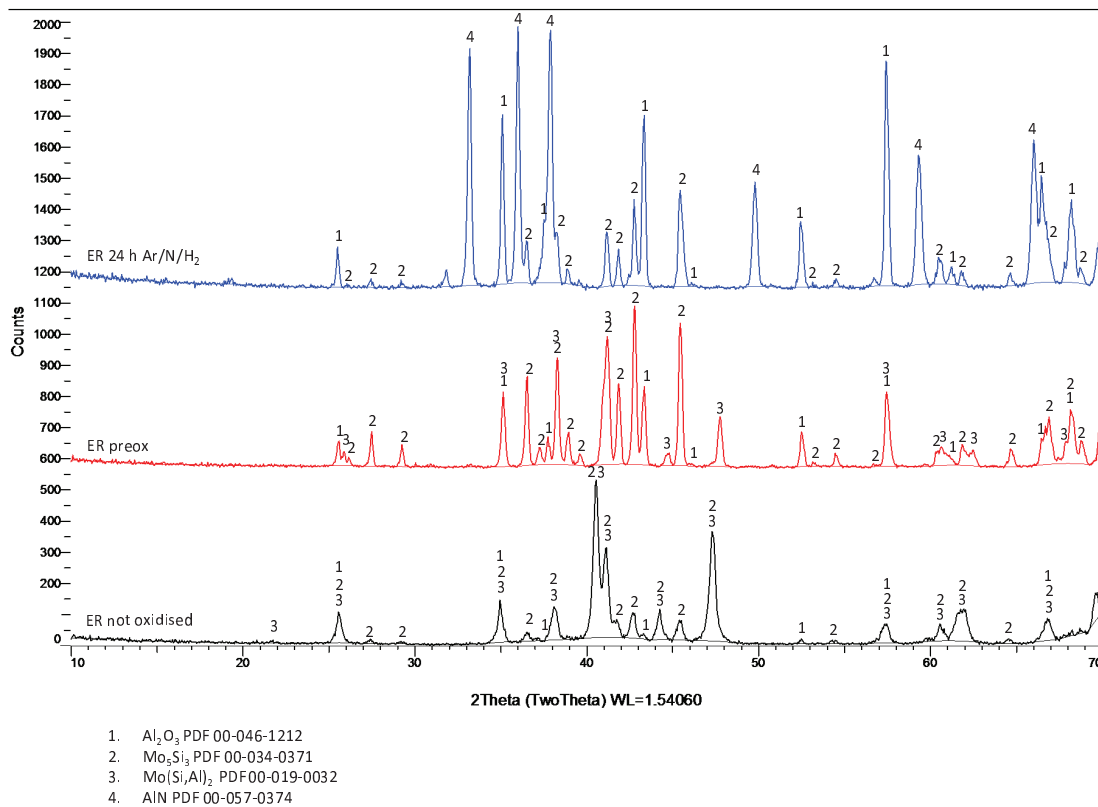


Figure 4.12: XRD analysis of ER exposed for 24 h in Argon, Nitrogen and Hydrogen, compared to preoxidised and not oxidised samples.

4.2.2 SEM cross section analysis

Figure 4.13 shows cross section SEM images of the ER samples exposed for 24 hours in argon, nitrogen and hydrogen. As in the previous section, the oxide layer appears to be consisting of two parts, one denser layer at the bottom and one more rough and porous at the top. However, in this case the rough part is more rough and appears to be falling off.

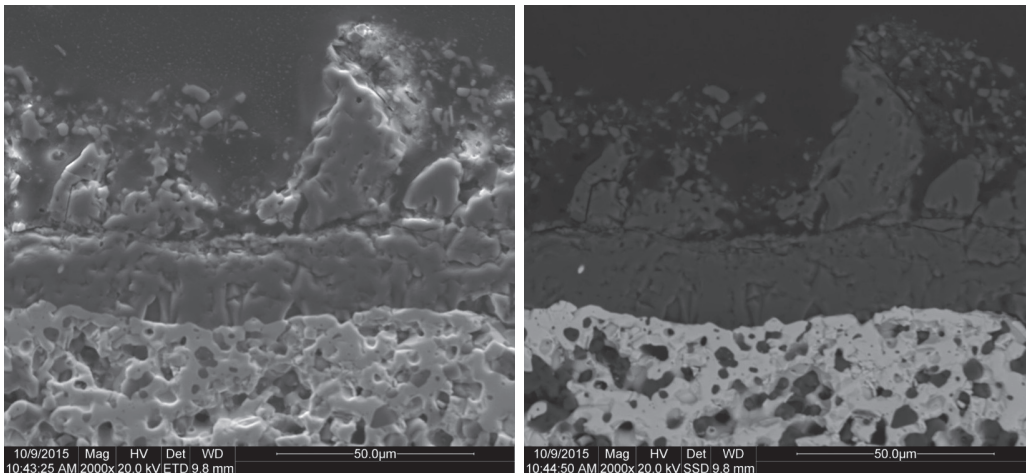


Figure 4.13: Cross section SEM images of ER after exposure for 24 h in argon, nitrogen and hydrogen. Left: Secondary electrons. Right: Backscattered electrons.

4.2.3 SEM surface analysis

Figure 4.14 shows SEM images of the surface of the samples. As can be seen, there is a network of bright rods as well as clusters. Figure 4.15 shows an image of needles formed on the surface. EDX analysis showed that these needles consists of pure alumina and the material underneath is a mix of alumina and AlN.

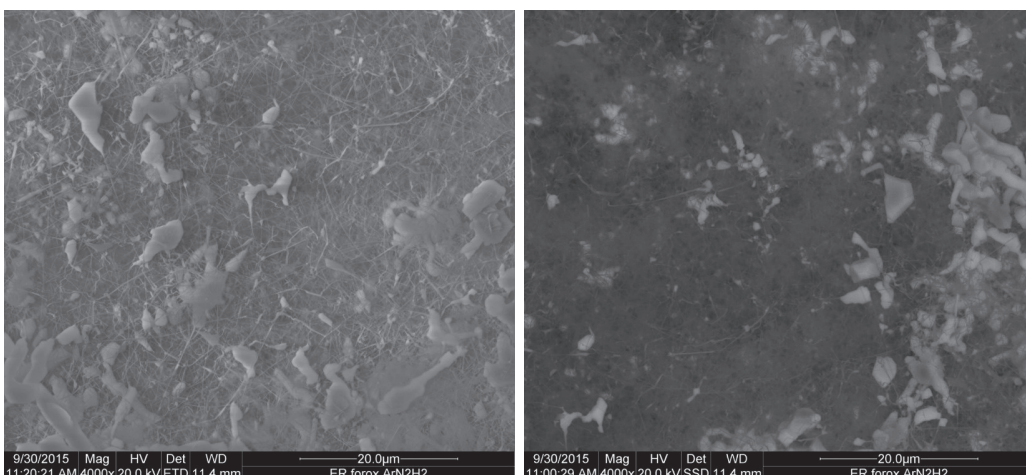


Figure 4.14: SEM surface images of ER after exposure for 24 h in argon, nitrogen and hydrogen. Left: Secondary electrons. Right: Backscattered electrons.

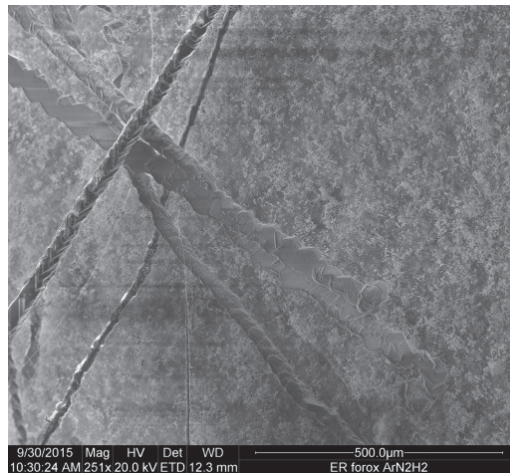


Figure 4.15: Secondary electron surface images of ER after exposure for 24 h in argon, nitrogen and hydrogen.

4.2.4 EDX mapping

Figure 4.16 shows an EDX mapping of an ER sample exposed for 24 hours in 1600°C. The oxide scale is clearly alumina, but there is a layer of nitride on top of the adherent oxide layer but beneath the rough top part of the oxide.

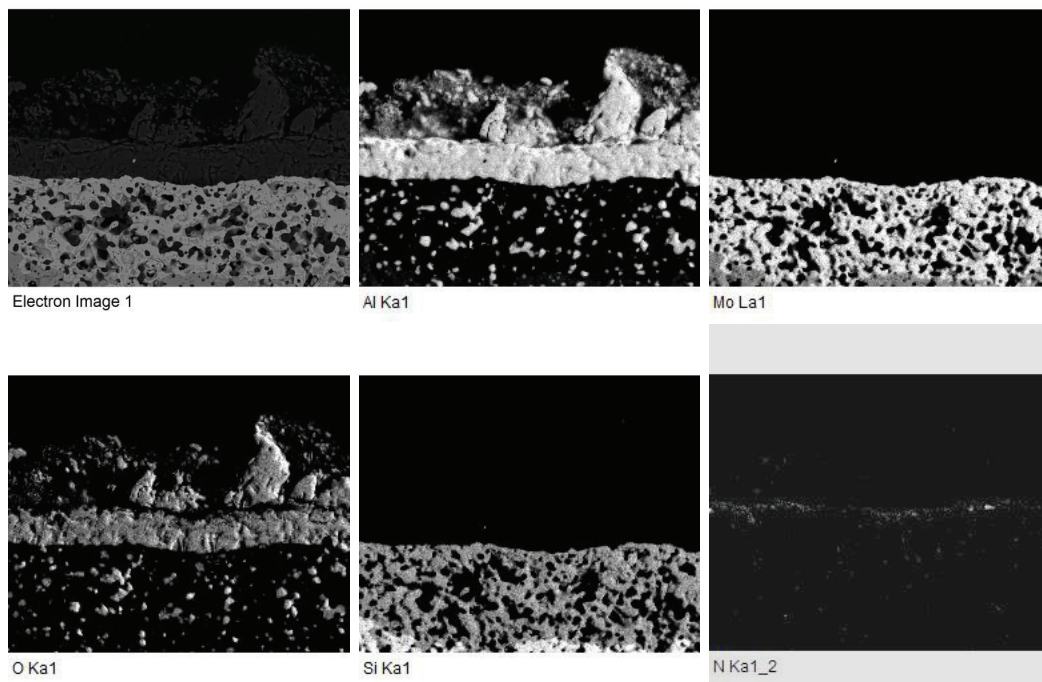


Figure 4.16: EDX mapping of a cross section from an ER sample exposed for 24 hours.

5

Discussion

Figure 5.1 shows a schematic overview of the oxide layers formed. Nitrides appear to be formed initially, but are then replaced by alumina. The alumina seems to be growing both inwards and outwards since the oxide thickens both above and below the nitride layer. The exact mechanism seems to be complicated, but there are some ideas of what is happening.

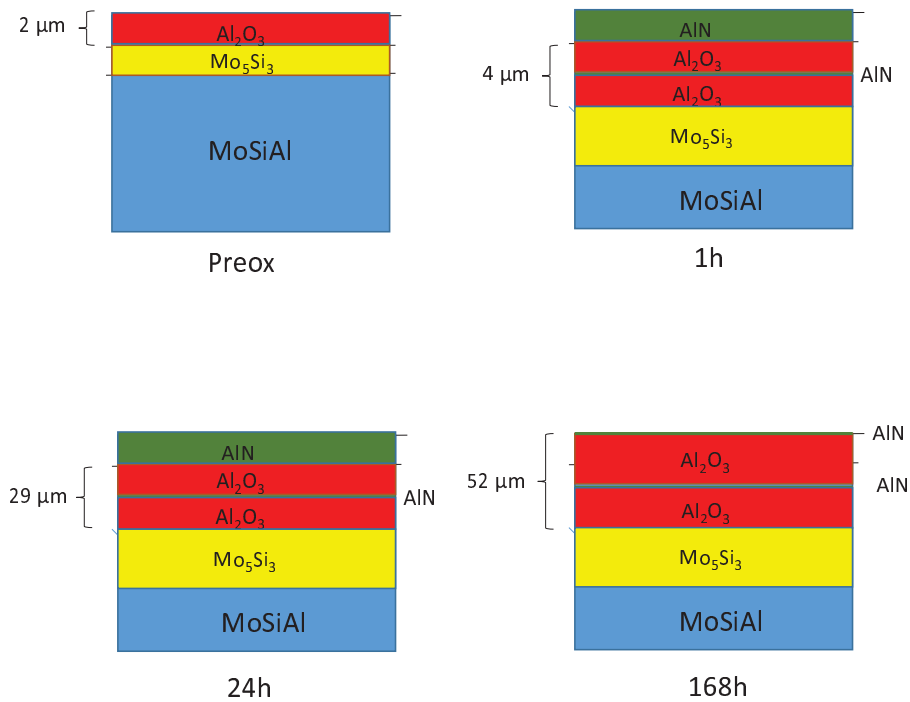


Figure 5.1: A schematic image of the oxide layers formed.

The initial formation of AlN could be explained by the fact that the atmosphere inside the tube is more reducing at lower temperature. The reason is that a lower temperature shifts the equilibrium of $\text{H}_2 + \text{O}_2 \leftrightarrow \text{H}_2\text{O}$ towards the right, which lowers the oxygen content. AlN is then formed on top of the alumina oxide layer resulting from the preoxidation. As the temperature rises it becomes possible for

AlN to oxidise into Al_2O_3 , which could help explain why there is no or very little AlN on the sample exposed for 168 hours. In section 3.2, it was mentioned that the oxygen partial pressure was about $4.4 \cdot 10^{-15}$ atm and the stability diagram in figure 5.2, created in the software FactSage, shows that alumina is indeed stable at those conditions. The alumina needles found on the surface of the samples could be the result of a volatile specie containing aluminium, which re-deposits on the surface. Two questions still remain: If AlN is formed during heating of the furnace, why would it not form when cooling, as the samples of 168 hours did not have AlN layer? And why is a tiny streak of AlN left in the middle of the oxide layer?

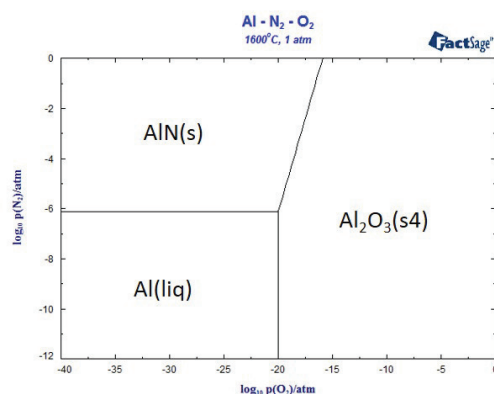


Figure 5.2: A stability diagram of AlN and Al_2O_3 created in FactSage.

These results are interesting, although more statistics are needed to confirm these results and there are unanswered questions. A first approach for continuing research would be to change the preparation method for the SEM cross section samples to be able to see the AlN layer and measure the thickness in order to get the full picture. Hopefully, avoid using water as a lubricant while polishing, might prevent the AlN from dissolving.

Also, as the samples cannot be inserted into the hot furnace, they have to be heated together with the furnace, meaning that the exposure time is not fully controlled. This is mostly important for the 1 hour exposure, as the heating and cooling time is much longer than the exposure time. As mentioned above, the nitrides are possibly formed during heating or cooling, indicating that this is an important factor. Future experiments could include checking if faster or slower heating/cooling has an impact on the result. It would be interesting to see what would happen after exposures during a longer time. Does the nitride disappear, or will the tiny streak inside the oxide remain?

5.1 Conclusion

From the exposures and analysis made in this project, it can be seen that nitrides are clearly formed when exposing ER in H_2 and N_2 at 1600°C. However, these appear only to form in the initial exposure time and seem to be overgrown by alumina as the samples are exposed for a longer time, which is indicated in both SEM and

XRD analysis. The nitride layer could then be found in the middle of the oxide layer. Finally, the exposure in argon, nitrogen and hydrogen gave similar results, although the oxidation appears to be faster and the alumina has not yet managed to cover the nitride layer.

Bibliography

- [1] Vasudevan A.K. and Petrovic J.J. A comparative overview of molybdenum disilicide composites. *Materials Science and Engineering*. 1992; 155: pp. 1-17.
- [2] Melsheimer S., Fietzek M., Kolarik V., Rahmel A. and Schiitze M. Oxidation of the Intermetallics MoSi₂ and TiSi₂ - A Comparison. *Oxidation of Metals*. 1997; 47(1/2)
- [3] Ingemarsson L., Halvarsson M., Hellström K., Jonsson T., Sundberg M., Johansson L-G. and Svensson J-E. Oxidation behavior at 300-1000°C of a (Mo,W)Si₂-based composite containing boride. *Intermetallics*. 2010; 18: pp. 77-86.
- [4] Sharif A. A.. High temperature oxidation of MoSi₂. *J Mater Sci*. 2010; 45: pp. 865–870
- [5] Ingemarsson, L. Oxidation of MoSi₂ based materials. Ph.D. Thesis. 2010 Chalmers University of Technology, Gothenburg, Sweden.
- [6] Massalski T.B. Binary Alloy Phase Diagrams, American Society for Metals, Metals Park, OH, USA,1990 p. 2664
- [7] P. J. Meschter, Low-Temperature Oxidation of Molybdenum Disilicide. *Metallurgical Transactions*. 1992; 23: pp. 1763-1772.
- [8] Bertiss, D. A., Cerchiara, R.R, Gulbransen E.A., Pettit F.S. and Meier G.H. Oxidation of MoSi₂ and comparison with other silicide materials. *Materials Science and Engineering*. 1992; 155: pp. 165-181
- [9] Cook J., Khan A., Lee E., Mahapatra R. Oxidation of MoSi₂-based composites. *Materials and Science Engineering*. 1992; 155: pp. 183-198.
- [10] Berkowitz-Mattuk, J.B, Rosetti, M. and Lee, D.W. The intermediate temperature oxidation behaviour of Molybdenum Disilicides. *Transactions of the Metallurgical Society of Aime*. 1965; 233: pp. 1093-1099
- [11] Chou, T.C., Nieh, T.G. New observations of MoSi₂ pest at 500°C. *Scripta Metallurgica et Materialia*. 1992; 26: pp. 1637-1642.
- [12] McKamey, C.G., Tortorelli, P.F., DeVan, J.H., Carmichael C.A. A study of pest oxidation in Polycrystalline MoSi₂. *Journal of Materials Research*. 1992; 7: pp. 2747-2755.
- [13] Rubish, V.O. Uber die Oxydation von Molybdändisilizid. *Ber. Dtsch. Kram. Ges.* 1964; 41: 120-127
- [14] Fitzer, E. Oxidation of Molybdenum Disilicide. *Ceram. Trans*. 1990; 10: 19-41.
- [15] Hansson, K. On the oxidation of MoSi₂ and (Mo,W)Si₂. Ph.D Thesis. Chalmers University of Technology 2003. Gothenburg.

- [16] Sharif A.A Effects of Re- and Al-alloying on mechanical properties and high-temperature oxidation of MoSi₂. *Journal of Alloy and Compounds*. 2012; 518: 22-26.
- [17] Hansson K., Halvarsson M., Tang J.E., Pompe R., Sundberg M. and Svensson J-E. *Journal of European Ceramic Society*. 2004; 24, pp. 3559-3573.
- [18] Bornstein N. Oxidation of advanced Intermetallic compounds. *Journal de Physique IV*. 1993; 3, 367-373.
- [19] Petrovic J.J. and Vasudevan A.K. Key developments in high temperature structural silicides. *Materials Science and Engineering*. 1999; A261: pp. 1-5.
- [20] Ingemarsson L., Hellström K., Canovic S., Jonsson T., Halvarsson M., Johansson L-G, Svensson J-E. Oxidation behavior of a Mo(Si,Al)₂ based composite at 900-1600°C in dry air. *Journal of Materials Science*. 2012; 48(4): pp. 1511-1523
- [21] Ingemarsson L., Hellström K., Johansson L-G, Svensson J-E and Halvarsson M. Oxidation behavior of a Mo(Si,Al)₂ based composite at 1500°C. *Intermetallics*. 2011; 19 (9): pp. 1319-1329.
- [22] Tabaru T., Shobu K., Hirai H. and Hanadab S. *Intermetallics*. 2003; 11: pp. 721-733.
- [23] Maruyama, T., Yanagihara, K. High temperature oxidation and pesting of Mo(Si,Al)₂. *Materials Science and Engineering*. 1997; 239-240: pp. 828-841.
- [24] Denny A. Jones. *Principles and Prevention of Corrosion*. 2 ed Prentice Hall, Inc. Simon & Schuster/ A Viacom company, 1996 Upper Saddle River, NJ.
- [25] Kofstad, Per; Johannesen, Øivind; Andersen, Arnfinn G. *Studies in Inorganic Chemistry*. 1989; 9: pp. 185-225
- [26] Karl Hauffe. *Oxidation of metals*. Plenum Press New York 1965.
- [27] John K. Tien. *Superalloys, Supercomposites and Superceramics*. Academic Press 1989, Boston. pp. 439-489
- [28] John K. Tien. *Superalloys, Supercomposites and Superceramics*. Academic Press 1989, Boston. pp. 671-696

A

Appendix I

For those interested, these sections provide some extra data, which was not included in the report.

A.1 Original XRD patterns

For clarity, the XRD patterns for each expoure are attached below. These images are easier to interpret as they are not scaled or altered in any way in order to fit onto the page.

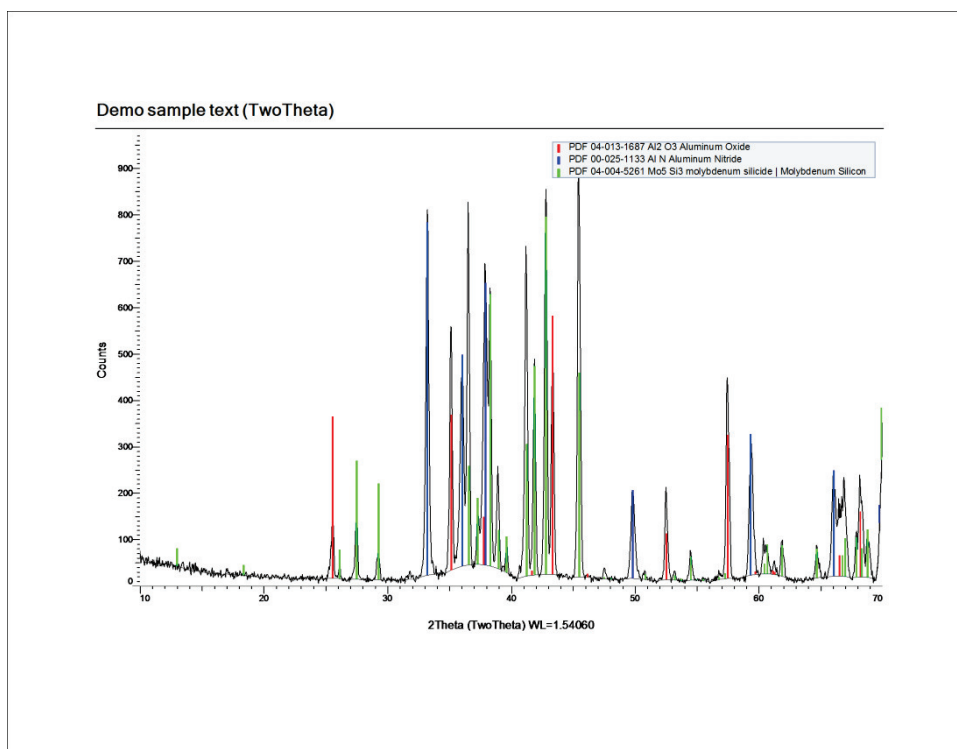


Figure A.1: XRD pattern of ER exposed for 1 hour.

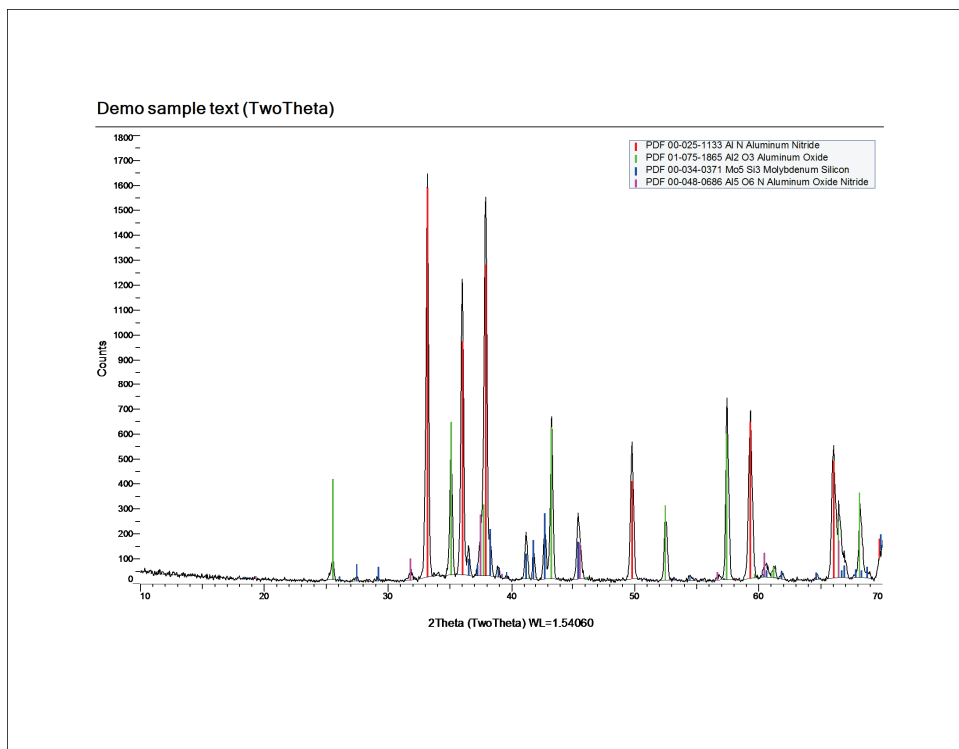


Figure A.2: XRD pattern of ER exposed for 24 hours.

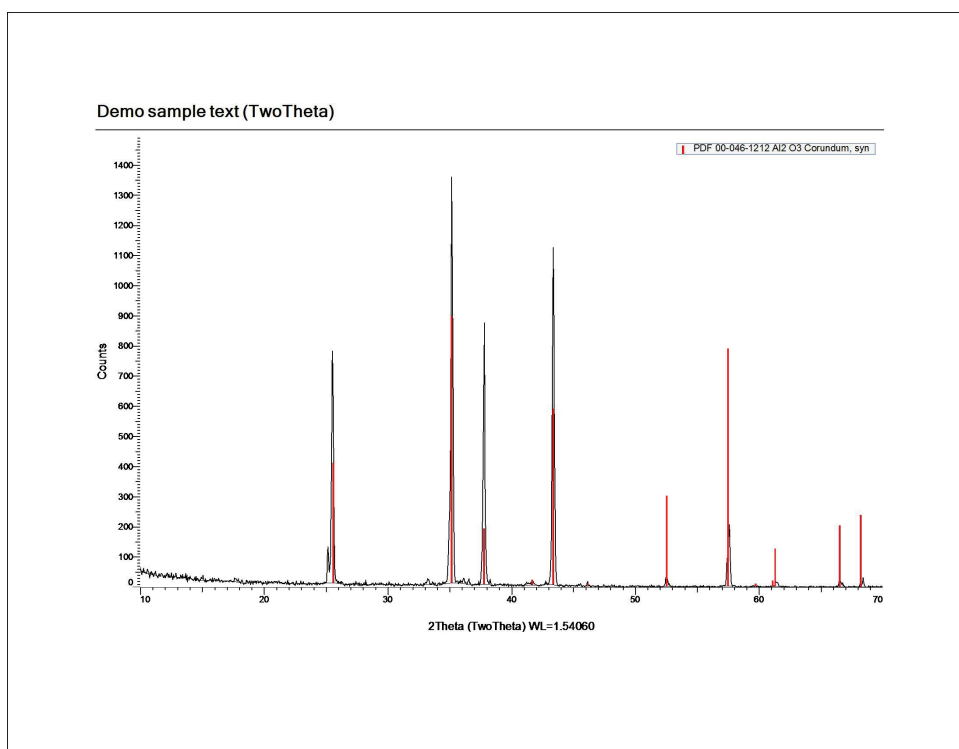


Figure A.3: XRD pattern of ER exposed for 168 hours.